UNABRIDGED MATERIALS AND METHODS

Phylogenetics

In order to understand the evolution of wing shape across the Bombycoidea, we sampled representatives of all Bombycoidea families. In total, the phylogenetic dataset included 57 species and one outgroup – the Lasiocampidae, the sister lineage to the Bombycoidea. Sampling was highest in the Saturniidae (25 sp.) and Sphingidae (24 sp.). Sequences were a mixture of previously sequenced individuals from prior studies (Breinholt et al., 2018; Rubin et al., 2018) and novel specimens (see Table S8). AHE sequences represented 53 species, while four species had their AHE loci mined from transcriptomic data (Table S8). Nineteen species were newly sequenced for this project, while 38 came from previously published datasets (Table S8). Species were chosen in order to capture the majority of the wing shape diversity throughout the Sphingidae and Saturniidae, based on availability in the collections at the Florida Museum of Natural History, Gainesville, FL, USA (FLMNH).

Specimens were obtained from historically preserved dry collections and molecular tissue collections stored at the Florida Museum of Natural History. DNA extraction from pinned museum specimens followed the protocol outlined in Hamilton et al. (2019). Field-collected specimens were stored in ≥95% ethanol, RNAlater (Sigma Aldrich, Saint Louis, MO, United States), or papered and dried with silica gel. Genomic DNA was extracted using OmniPrep Genomic DNA Extraction Kits (G-Biosciences, St. Louis, MO, USA) and DNeasy Blood and Tissue Kits (Qiagen, Valencia, CA, USA). DNA concentration was evaluated through agarose gel electrophoresis and fluorometry using a Qubit 2.0 (Invitrogen, Thermo Fisher Scientific, Carlsbad, CA, USA).

We used the Bombycoidea-specific 'BOM1' Anchored Hybrid Enrichment (AHE) probe set to target 571 loci (Hamilton et al., 2019). AHE is a targeted-sequencing methodology designed to capture hundreds of unique orthologous loci (i.e., single copy, phylogenetically-informative markers) from across the genome, for resolving both shallow and deep-level evolutionary relationships (Lemmon et al., 2012; Breinholt et al., 2018).

Library preparation, hybridization enrichment, and Illumina HiSeq 2500 sequencing (PE100) was carried out at RAPiD Genomics (Gainesville, FL, USA). Specimen wing vouchering and tissue storage methods follow Cho et al. (2016). All DNA extracts and specimens preserved in ethanol, RNAlater, or those freshly papered were stored at -80°C at the FLMNH, McGuire Center of Lepidoptera and Biodiversity (MGCL). Historically preserved dry collection specimens were kept in their traditional storage method - pinned in their tray or papered in a box, at the MGCL.

The bioinformatics pipeline of Breinholt et al. (2018) was used to clean and assemble raw Illumina reads for each AHE locus. The pipeline uses a probe-baited iterative assembly that extends beyond the probe region, checks for quality and cross contamination due to barcode leakage, removes paralogs, and returns a set of aligned orthologs for each locus and taxon of interest. To accomplish these tasks, the pipeline uses the *Bombyx mori* genome (Xia et al., 2004), and the BOM1 AHE reference library. Previously published scripts (Breinholt et al., 2018) and instructions (Hamilton et al., 2019) on the pipeline are available in Dryad (https://doi.org/10.5061/dryad.5df18fp).

Loci for phylogenetic analysis were selected by applying a cutoff of ≥60% sampled taxa recovery (i.e., for a locus to be included in the analysis, the locus had to be recovered in at least

60% of the sampled taxa). The pipeline evaluates density and entropy at each site of a nucleotide sequence alignment. We elected to trim with entropy and density cutoffs only in flanking regions, allowing the probe region (exon) to be converted into amino acid sequences. For a site (outside of the probe region) to remain, that site must then also pass a 60% density and 1.5 entropy (saturation) cutoff, rejecting sites that fail these requirements. A higher first value (60) increases the coverage cutoff (e.g., a site is kept if 60% of all taxa are represented at that site). A higher second value (1.5) increases the entropy cutoff (i.e., entropy values represent the amount of saturation at a site); sites with values higher than 1.5 possess higher saturation and are thus deleted). Following Hamilton et al. (2019), we built and utilized a Pr+Fl dataset; a concatenated dataset consisting of 605 probe regions + a flanking supermatrix for phylogeny inference. The final dataset comprised 606 loci and 222,369 bp.

AliView v1.18 (Larsson, 2014) was used to translate the nucleotides to amino acids, check for frame shifts, and edit sequencing errors or lone/dubious indels. Because flanking sequences are generally non-coding and sites have been deemed homologous, the flanking sequences (i.e., those before and after the probe regions), were separated from the exons, then combined and treated together as an independent partition. Due to the filtering steps in the bioinformatics pipeline (i.e., site orthology, and density and saturation evaluation), the flanking partition can be viewed as a SNP supermatrix, where each site is homologous and independent, but uninformative sites, saturated sites, or sites with large amounts missing data removed. Specimens whose AHE loci were mined from transcriptomes did not have flanking data due to the nature of transcriptomic data.

A concatenated supermatrix was assembled using FASconCAT-G v1.02 (Kueck and Longo, 2014). Phylogenetic inference was performed in a maximum likelihood (ML) framework using IQ-TREE v1.5.3 (Nguyen et al., 2015). Within this framework we searched for the most appropriate model of nucleotide substitution, as well as 1000 random addition sequence (RAS) replicates, and 1000 replicates each for both ultrafast bootstraps (UFBS) and SH-aLRT tests to find the "best" tree and node support. We classified nodes as well-supported if they were recovered with support values of UFBS ≥ 95 and SH-aLRT ≥ 80 (Minh et al., 2013; Nguyen et al., 2015). All branch length estimates are in units of substitutions per site. In the ultrametric tree used for analyses, the branch lengths were scaled relative to each other. All pipeline steps and phylogenomic analyses were conducted on the University of Florida HiPerGator HPC (http://www.hpc.ufl.edu/). All alignment FASTA files, partition files, tree files, and other essential data files used for phylogenetic inference are available as supplementary materials on Dryad.

The tree was dated using the chronopl function in the ape (version 5.3) R package (Paradis and Schliep, 2019). We assigned a minimum and maximum age to nodes 58, 59, 61, 62, 63, 88, and 112 (see Fig. S2B) based on the dates of the corresponding nodes in a recently published fossil-calibrated Lepidoptera tree (Kawahara et al., 2019).

Museum specimen imaging

Specimens from the FLMNH collections were imaged using a 60 mm lens (Canon, Tokyo, Japan) mounted to a Canon EOS 7D camera (Canon, Tokyo, Japan). See Table S9 for details on the number and sex of specimens imaged per species. For this analysis, male specimens were

analyzed when available (53 of 57 species). We chose to focus on males because they are known to exhibit higher flight activity in comparison to females (Gilchrist, 1990; Le Roy et al., 2019).

Body and wing measurements

The body and wing morphology was digitized from museum images using the StereoMorph package (version 1.6.2) (Olsen and Westneat, 2015) in R (version 3.4.2; The R Foundation for Statistical Computing). Eight landmarks were digitized to characterize body size and shape (Fig. S1), and a series of third order Bézier curves were used to outline the right forewing and hindwing (Fig. S1). The curves were then resampled using the StereoMorph package to generate 50 evenly spaced points (semilandmarks) around the wing perimeter. For species with multiple individuals, the species average shape and size was obtained by averaging the aligned position of each landmark (or semilandmark).

Wing measurements for all species began by re-orienting each wing to a comparable orientation consistent with what is known of flight position. The forewing was rotated so its long axis was perpendicular to the long axis of the body. In species of Sphingidae, the long axis of the hindwing was also rotated to be perpendicular to the long axis of the body, as is its approximate orientation during flight. The hindwing of Saturniidae and the "other bombycoid families" were kept in the same orientation of dried museum specimens, which is the approximate orientation during flight and provides a consistent and comparable orientation across species.

Next, we created a combined wing outline from the non-overlapping portions of the rotated forewing and hindwing. The rotated forewing and hindwing were positioned relative to each other based on their known attachment points to the thorax, which we digitized. The combined wing shape represents the wing shape used for force generation, and is therefore the most functionally relevant shape. The X and Y points of the combined wing outline were then resampled to generate 75 evenly spaced points.

We estimated specific forewing, hindwing, and combined wing shape traits in Matlab (version R2018b – 9.5.0.944444). For both wings, we measured wing length (R) as the distance between the minimum and maximum value of the wing outline. All additional wing parameters (S, AR, and $\hat{r}_2$) were calculated following Ellington (1984a) for each wing. We also calculated wing loading for the combined wing shape, W_s, by dividing total body mass (m_t) by the total area of the outline of the overlapping fore and hindwing (removing any portion of the hindwing that overlaps with the forewing). We use a morphology based estimate of wing beat frequency (n) using an equation derived through dimensional analysis of insect body mass and wing area (Table 1; Deakin, 2010). Finally, body mass specific mean inertial power of the wing pair (P_{acc}) was calculated (see Table S1) following published methods (Ellington, 1984b).

Figure S1. Summary of body landmarks and exemplar wing digitizing methodology. Eight landmarks (blue points) capture body size and position of wings on the body: the tip of the head (i), the caudal tip of the abdomen (ii), the junction between the head and thorax (iii), and the junction between the thorax and abdomen (iv), the widest points of the thorax (v), the widest points of the abdomen (vi), the rostral and caudal positions of the forewing (vii) and hindwing bases. Each wing was then outlined using a series of Bezier curves. The points outlining the wing (purple) in this figure do not represent the semi-landmarks, but rather the points of the sequential curves used to outline the wing. Each curve was free to vary in perimeter length, and, typically, more points were used to generate the outline around more complex regions of the wing (see distal tip versus leading edge). The final curve was then resampled to generate the evenly distributed semi-landmarks (see methods).

The estimation of body and wing mass

The calculation of W_s and estimation of n and P_{acc} depend on body and wing mass. Thus, we used a set of live adult specimens to ensure accurate estimations of mass. We first weighed a total of 71 live specimens representing 8 and 13 species of Sphingidae and Saturniidae,

respectively (Table S5). Then we predicted body mass from morphology by modelling the body as three ellipsoids: one for the head, thorax, and abdomen. The length and width of each body segment were measured as the distance between the minimum and maximum value for that segment. The width of the head was assumed to be equal to its length. The dorso-ventral depth of every segment was assumed to be equal to its width. The assumption that the density of each body segment was equal to 0.6 x water density resulted in the estimation of body mass predicted from morphology to deviate from actual mass by 1.5 ± 31.6 % (mean ± s.d.) across all individuals and species (Fig. S6A).

Next, to estimate the mass of the forewing and hindwing of museum specimens, we used the same set of 71 living specimens to develop a relationship between log wing area and log wing mass that assumes wing thickness is constant. For both wings, we found a significant relationship with an r^2 greater than 0.89 (Fig. S6B-C; forewing: r^2>0.89, p <10^{-34}, F = 592; hindwing: r^2>0.92, p <10^{-39}, F = 834). From these relationships, forewing and hindwing mass were estimated as $m_{fw} = 10^{(0.965\log(S_{fw}))+1.417}$ and $m_{hw} = 10^{(1.068\log(S_{hw}))+1.535}$, respectively. The estimate deviated from actual mass across all individuals of all species of -3.5 ± 27.6% and -4.4 ± 32.5% for the forewing and hindwing, respectively.

Morphometric analysis of wing shape

To examine the variation in forewing, hindwing, and combined wing shape while accounting for phylogeny, we conducted a phylogenetic principal components analysis (pPCA) (Revell, 2009). A pPCA finds the dimensions of wing shape that maximize the covariance of the component shape variables but corrects the covariance with a relatedness matrix that takes into account

the shared evolutionary history of the samples. For each species, the mean wing semilandmarks were aligned by Procrustes superimposition to obtain size and orientation corrected Procrustes coordinates (implemented with *gpagen* function in Geomorph R package (version 3.1.2)). Next, the pPCA was conducted on the Procrustes coordinates for each species (implemented with the *phyl.pca* function in the R package phytools (version: 0.6-60) (Revell, 2012)). We then projected wing shape back on to the first four pPC axes (Olsen, 2017). To test if clades were significantly clustered in four dimensional pPC morphospace, for each wing shape, we conducted a MANOVA where the pPC scores of pPC1, 2, 3, and 4 were used as the response variable and clade (hawkmoths, silkmoths, or other bombycoid (O.B.) lineages) was the factor.

Evolutionary analyses

In order to determine how disparity (trait variance) of each morphological trait evolved relative to the divergence of the sister families, we conducted a disparity through time (DTT) analysis (Harmon et al., 2003) on forewing, hindwing, and combined wing shape as well as combined wing AR, $\hat{r}_2$, W_s, relative wing area (S/m_t), and n. For each trait at every time step, the analysis determines the average disparity of each subclade (hawkmoths, silkmoths, and other bombycoid (O.B.) families) in comparison to the total disparity across all species (Harmon et al., 2003). Under Brownian motion (BM), relative subclade disparity will show a relatively linear decline over evolutionary time. Extant functional disparity could also evolve recently in time, which is seen when relative subclade disparity is greater than that under BM in recent time and suggests that traits are evolving around an adaptive peak (Lopez-Fernandez et al., 2013). Alternatively, relative subclade disparity being lower than that under BM is a sign that the

evolutionary accumulation of morphological variation occurred early in evolutionary history (Harmon et al., 2003). In order to quantify differences in relative subclade disparity relative to trait evolution under BM, we calculated a morphological disparity index (MDI), which is the area between the observed DTT curve and DTT curves of trait evolution simulated under BM, and is expected to be zero under BM. We performed 1000 simulations for each trait DTT analysis.

Next, we aimed to determine if discrete adaptive shifts in wing morphology were associated with the separation between the hawkmoths and silkmoths. To do this, we performed a maximum likelihood estimation of the presence of shifts and, if they existed, their positions using the PhylogeneticEM R package (Bastide et al., 2018). We tested for the presence of adaptive shifts for the combined wing shape as well as combined wing AR, $\hat{r}_2$, W_s, relative wing area (S/m_t), and n.

Finally, to further determine the most likely processes of trait evolution, we compared the fit of different models of trait evolution. We used the mvMORPH R package (Clavel et al., 2015) to fit ten different evolutionary models to each trait. We fit a single rate BM, a single-regime (Ornstein-Uhlenbeck) OU, and an early burst (EB) model. We also fit three multi-regime models for both BM and OU processes that allowed: (1) all three groups (hawkmoths, silkmoths, and other bombycoid families) to differ in trait evolution, (2) silkmoths to differ from the other two groups (hawkmoths and O.B. families), and (3) hakwmoths to differ from the other two groups. Finally, we also fit a multi-peak OU model that represents the adaptive shifts recovered from the PhyloEM models above. Each model was fit to the following morphological traits: the pPC scores for the dominant axes of combined wing shape and combined wing AR, $\hat{r}_2$, W_s, relative wing area (S/m_t), and n. The dominant axes for wing shape were determined

using the broken sticks method implemented in the bsDimension function of the PCDimension R package V 1.1.11 (Wang et al., 2018). The different model fits were compared using sample-size corrected Akaike Information Criterion scores (AICc).

REFERENCES

Bastide, P., Ane, C., Robin, S. and Mariadassou, M. (2018). Inference of Adaptive Shifts for Multivariate Correlated Traits. *Systematic Biology* **67**, 662-680.

Breinholt, J. W., Earl, C., Lemmon, A. R., Lemmon, E. M., Xiao, L. and Kawahara, A. Y. (2018). Resolving Relationships among the Megadiverse Butterflies and Moths with a Novel Pipeline for Anchored Phylogenomics. *Systematic Biology* **67**, 78-93.

Cho, S., Epstein, S. W., Mitter, K., Hamilton, C. A., Plotkin, D., Mitter, C. and Kawahara, A. Y. (2016). Preserving and vouchering butterflies and moths for large-scale museum-based molecular research. *Peerj* **4**.

Clavel, J., Escarguel, G. and Merceron, G. (2015). mvMORPH: an R package for fitting multivariate evolutionary models to morphometric data. *Methods in Ecology and Evolution* **6**, 1311-1319.

Deakin, M. A. B. (2010). Formulae for insect wingbeat frequency. *Journal of Insect Science* **10**.

Ellington, C. P. (1984a). The Aerodynamics of Hovering Insect Flight .2. Morphological Parameters. *Philosophical Transactions of the Royal Society of London Series B-Biological Sciences* **305**, 17-40.

Ellington, C. P. (1984b). The Aerodynamics of Hovering Insect Flight .6. Lift and Power Requirements. *Philosophical Transactions of the Royal Society of London Series B-Biological Sciences* **305**, 145-181.

Gilchrist, G. W. (1990). The Consequences of Sexual Dimorphism in Body Size for Butterfly Flight and Thermoregulation. *Functional Ecology* **4**, 475-487.

Hamilton, C. A., St Laurent, R. A., Dexter, K., Kitching, I. J., Breinholt, J. W., Zwick, A., Timmermans, M., Barber, J. R. and Kawahara, A. Y. (2019). Phylogenomics resolves major relationships and reveals significant diversification rate shifts in the evolution of silk moths and relatives. *BMC Evol Biol* **19**, 182.

Harmon, L. J., Schulte, J. A., Larson, A. and Losos, J. B. (2003). Tempo and mode of evolutionary radiation in iguanian lizards. *Science* **301**, 961-964.

Kawahara, A. Y., Plotkin, D., Espeland, M., Meusemann, K., Toussaint, E. F. A., Donath, A., Gimnich, F., Frandsen, P. B., Zwick, A., dos Reis, M. et al. (2019). Phylogenomics reveals the evolutionary timing and pattern of butterflies and moths. *Proceedings of the National Academy of Sciences of the United States of America* **116**, 22657-22663.

Kueck, P. and Longo, G. C. (2014). FASconCAT-G: extensive functions for multiple sequence alignment preparations concerning phylogenetic studies. *Frontiers in Zoology* **11**.

Larsson, A. (2014). AliView: a fast and lightweight alignment viewer and editor for large datasets. *Bioinformatics* **30**, 3276-3278.

Le Roy, C., Debat, V. and Llaurens, V. (2019). Adaptive evolution of butterfly wing shape: from morphology to behaviour. *Biological Reviews* **94**, 1261-1281.

Lemmon, A. R., Emme, S. A. and Lemmon, E. M. (2012). Anchored Hybrid Enrichment for Massively High-Throughput Phylogenomics. *Systematic Biology* **61**, 727-744.

Lopez-Fernandez, H., Arbour, J. H., Winemiller, K. O. and Honeycutt, R. L. (2013). Testing for Ancient Adaptive Radiations in Neotropical Cichlid Fishes. *Evolution* **67**, 1321-1337.

Minh, B. Q., Nguyen, M. A. T. and von Haeseler, A. (2013). Ultrafast Approximation for Phylogenetic Bootstrap. *Molecular Biology and Evolution* **30**, 1188-1195.

Nguyen, L. T., Schmidt, H. A., von Haeseler, A. and Minh, B. Q. (2015). IQ-TREE: A Fast and Effective Stochastic Algorithm for Estimating Maximum-Likelihood Phylogenies. *Molecular Biology and Evolution* **32**, 268-274.

Olsen, A. M. (2017). Feeding ecology is the primary driver of beak shape diversification in waterfowl. *Functional Ecology* **31**, 1985-1995.

Olsen, A. M. and Westneat, M. W. (2015). StereoMorph: an R package for the collection of 3D landmarks and curves using a stereo camera set-up. *Methods in Ecology and Evolution* **6**, 351-356.

Paradis, E. and Schliep, K. (2019). ape 5.0: an environment for modern phylogenetics and evolutionary analyses in R. *Bioinformatics* **35**, 526-528.

Revell, L. J. (2009). Size-Correction and Principal Components for Interspecific Comparative Studies. *Evolution* **63**, 3258-3268.

Revell, L. J. (2012). phytools: An R package for phylogenetic comparative biology (and other things). *Methods Ecol. Evol.* **3**, 217-223.

Rubin, J. J., Hamilton, C. A., McClure, C. J. W., Chadwell, B. A., Kawahara, A. Y. and Barber, J. R. (2018). The evolution of anti-bat sensory illusions in moths. *Science Advances* **4**.

Wang, M., Kornblau, S. M. and Coombes, K. R. (2018). Decomposing the Apoptosis Pathway Into Biologically Interpretable Principal Components. *Cancer Informatics* **17**.

Xia, Q. Y., Zhou, Z. Y., Lu, C., Cheng, D. J., Dai, F. Y., Li, B., Zhao, P., Zha, X. F., Cheng, T. C., Chai, C. L. et al. (2004). A draft sequence for the genome of the domesticated silkworm (Bombyx mori). *Science* **306**, 1937-1940.

Supplemental Figures

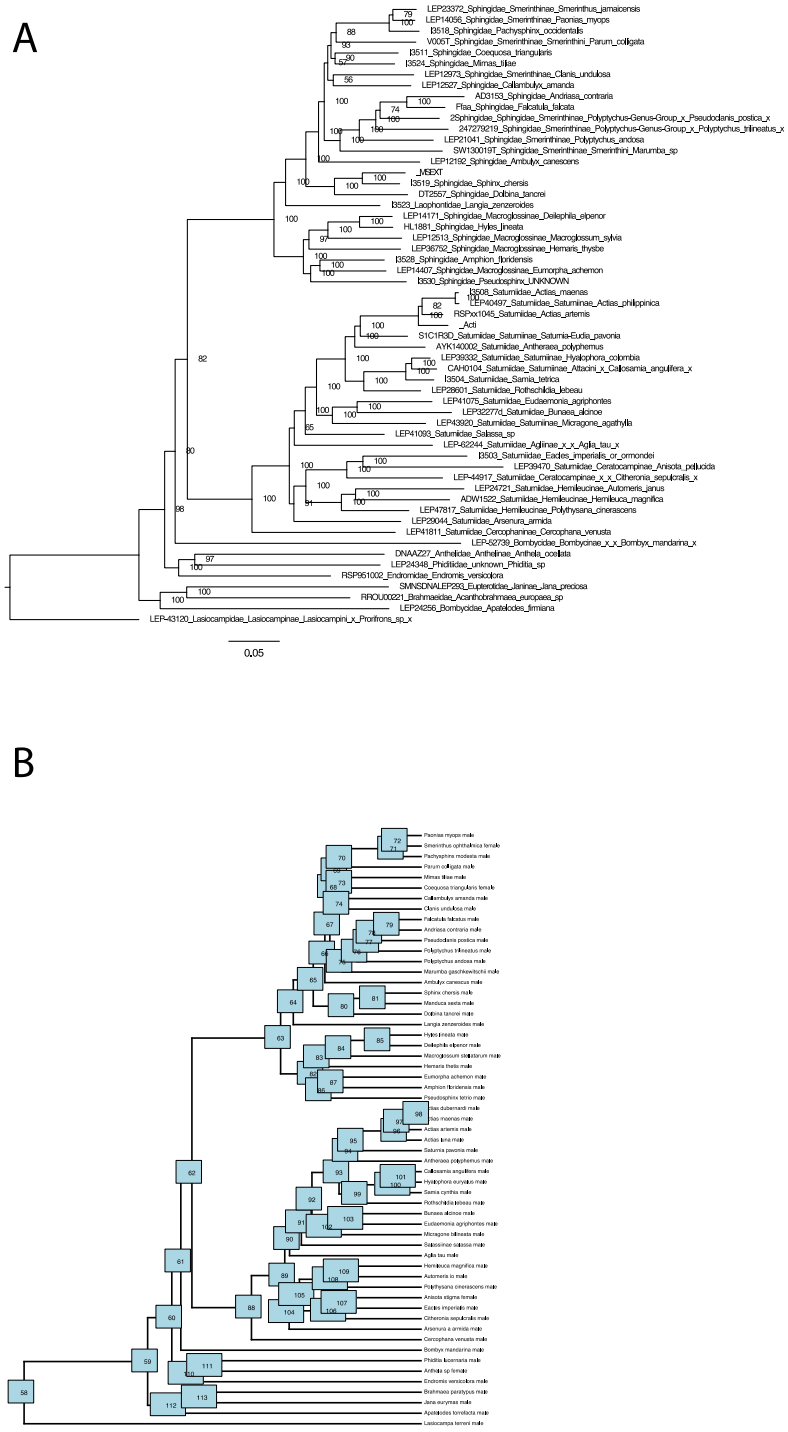

Fig. S2. (A) Bombycoid phylogeny with bootstrap values for each node. (B) Key for phylogeny node labels. Numeric labels for each node of the phylogeny are listed in their corresponding location (blue boxes).

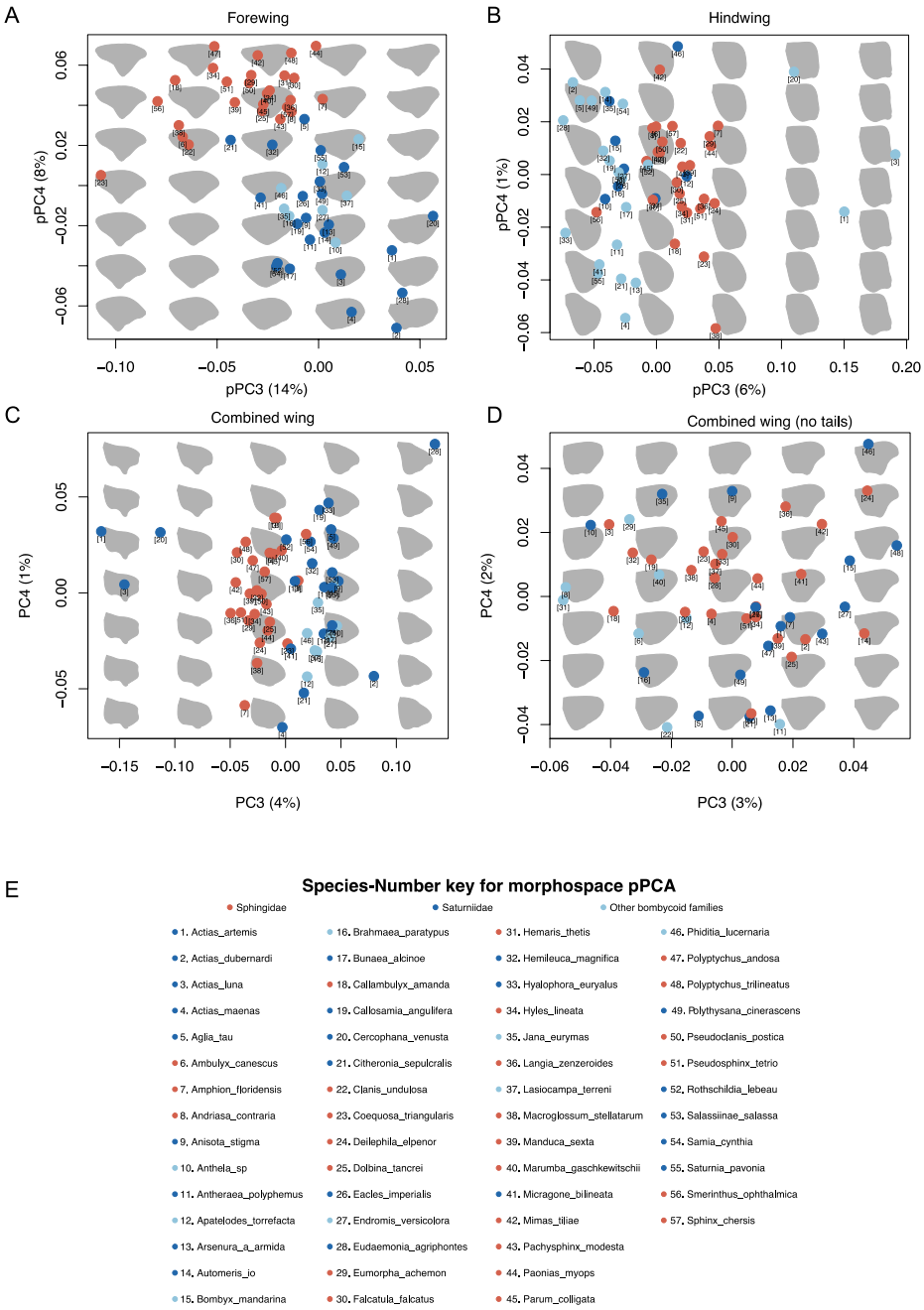

Figure S3. Morphospace across the pPC3 and pPC4 axes for the (A) forewing, (B) hindwing, (C) combined wing, and (D) combined wing after the removal of tailed species. (E) Key for species names in morphospace. This figure contains the number and corresponding scientific name of each species in morphospace. These numbers are used in Fig. 1.

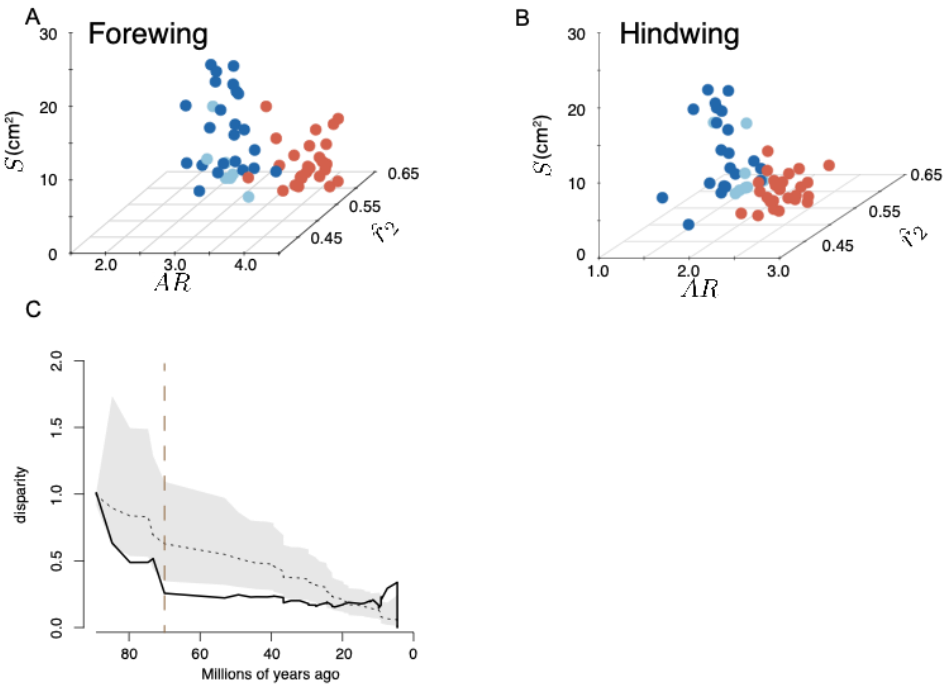

Fig. S4. Morphospace of functional wing variables.
Wing area (S), aspect ratio (AR), radius of second moment of wing area ($\hat{r}_2$) plotted in 3-D morphospace for the forewing (A) and hindwing (B). A DTT plot for combined wing shape after removing tailed species (C).

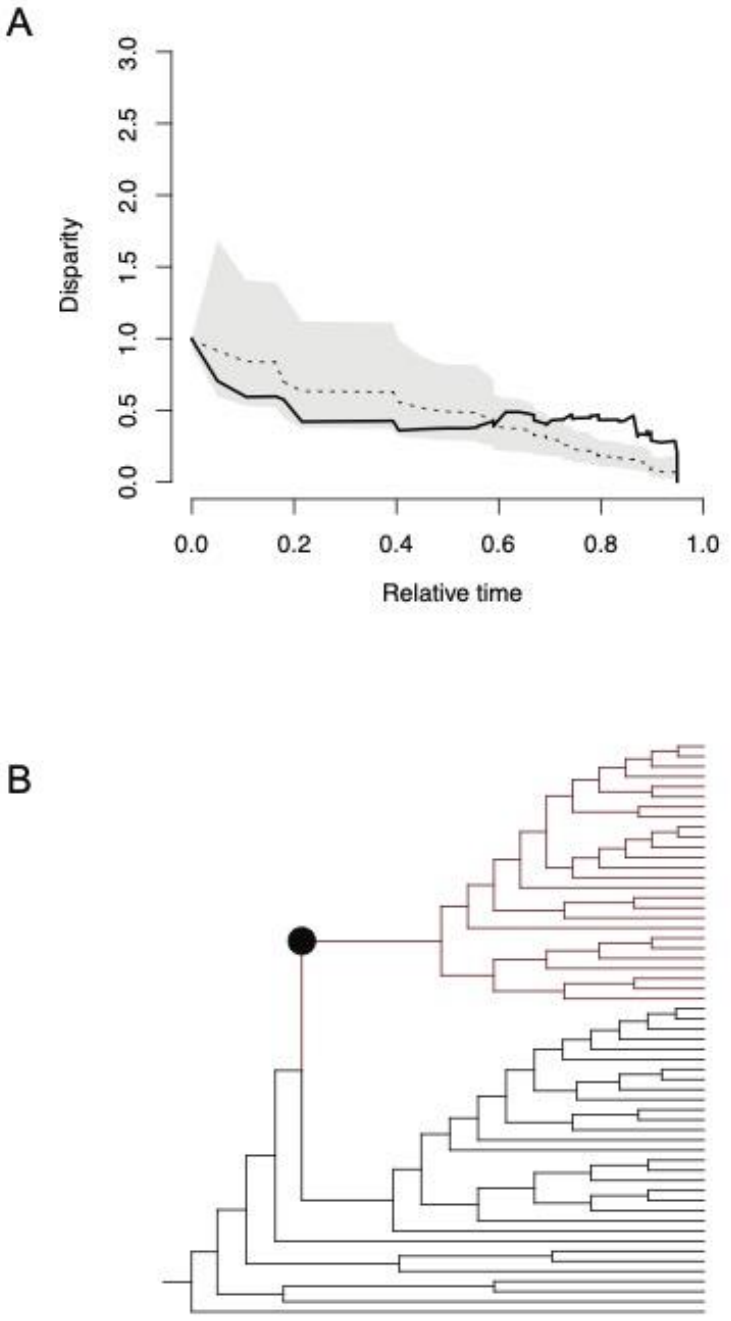

Fig. S5. Disparity through time and adaptive shift of multiple wing variables.
The disparity through time (A) and position of an adaptive shift when multiple wing variables are analyzed together. Variables in the model are the z-scores of wing beat frequency, radius of the second moment of area, aspect ratio, and relative wing size.

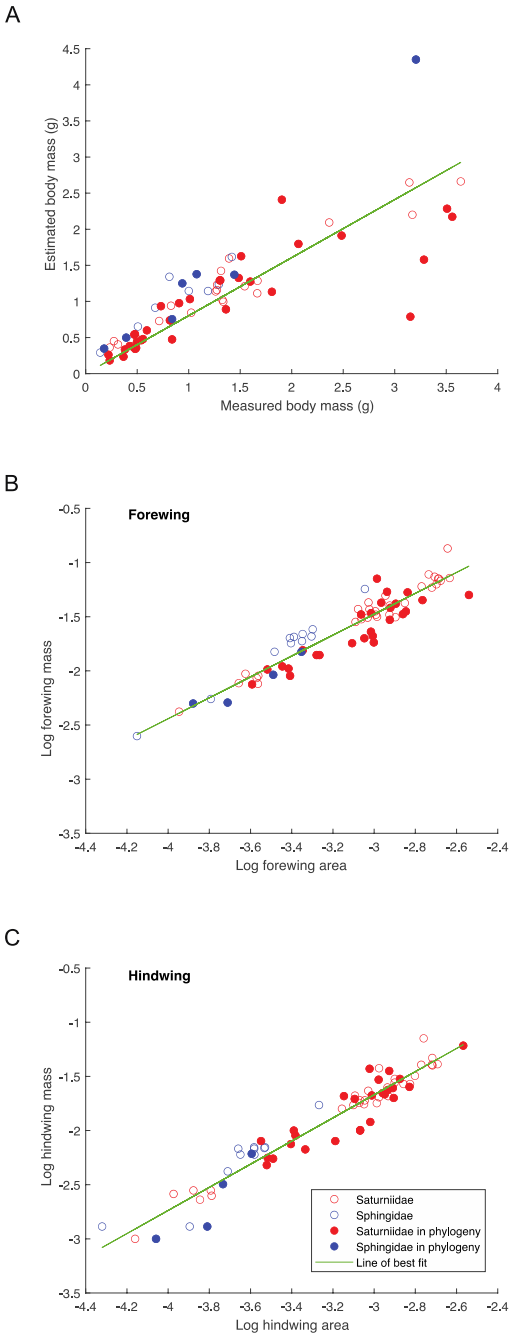

Fig. S6. The relationships between estimated and measured body mass (A) as well as the scaling relationships between the wing area and mass for both the forewing (B) and hindwing (C) The regression between measured and estimated body mass is significant ($r^2 = 0.712$, $p < 10^{-35}$).

Table S1.

Term	Symbol or abbreviation	Formula
Forewing	fw	
Hindwing	hw	
Combined wing	cw	
Forewing mass	m_{fw}	$10^{(0.9647 \times \log(S_{fw}))+1.4170}$
Hindwing mass	m_{hw}	$10^{(1.0681 \times \log(S_{hw}))+1.5348}$
Combined wing mass	m_{cw}	$m_{fw} + m_{hw}$
Body mass	m_b	
Total (body + wings) mass	m_t	$m_b + 2m_{cw}$
Wing area	S	
Body length	l_b	
Abdomen length	l_{abd}	
Fraction of body length occupied by abdomen	$\hat{l}_{abd}$	l_{abd}/l_b
Fraction of body length occupied by thorax	$\hat{l}_{tho}$	l_{tho}/l_b
Wing length	R	
Mean chord length of wing	$\bar{c}$	
Aspect ratio	AR	R^2/S
Wing loading	W_s	$m_t\ /\ (2S)$
Relative wing area	S/m_t	S/m_t
Nondimensional radius of second moment of area	$\hat{r}_2$	$\sqrt{\int_0^1 \hat{c}\hat{r}^2 d\hat{r}}$
Wingbeat frequency	n	$187 m_t^{0.3} S^{-0.7}$
Body mass-specific mean inertial power	P_{acc}	$8\pi^2 \phi_{p-p}^2 n^3 R^2 \hat{r}_2 m_w/m_t$
Million years ago	MYA	
Other Bombycoid lineages	O.B.	
n^{th} axis of the phylogenetic principal components	pPCn	

Table S1. List of symbols

	Forewing	Hindwing	Combined wing	Combined wing (no tailed species)
pPC	**% variace explained**	**% variace explained**	**% variace explained**	**% variace explained**
1	44.09582	61.52347	51.37017	86.8765
2	23.83015	27.74404	40.95677	5.196338
3	14.03427	6.240723	3.615423	2.595809
4	7.792455	1.393257	1.273619	1.61497
5	3.291639	0.7216899	0.6714563	0.9806427
6	1.770288	0.5494574	0.6268477	0.6797778
7	0.9731021	0.4731804	0.3054692	0.4316847
8	0.9023281	0.3032473	0.2673208	0.352565
9	0.6639413	0.1996426	0.2275375	0.2363785
10	0.4699692	0.1659755	0.1442992	0.2030086
11	0.4319547	0.1404104	0.08671484	0.1535963
12	0.3761678	0.1309702	0.06399783	0.1220696
13	0.2584309	0.08712083	0.05808622	0.1024811
14	0.2046103	0.06048337	0.05702806	0.08389669
15	0.1791709	0.04674457	0.05165864	0.06666559
16	0.1364759	0.04135925	0.03711033	0.05636093
17	0.1095621	0.02633463	0.03254008	0.03873215
18	0.06996234	0.02419724	0.02680381	0.02998763
19	0.06870354	0.0179083	0.02162276	0.02854512
20	0.04532666	0.017088	0.01678744	0.02226583
21	0.04341963	0.01574192	0.0125108	0.01996837
22	0.03460411	0.01243637	0.01089621	0.01530132
23	0.0326272	0.01023976	0.009526719	0.0149843
24	0.03039895	0.008445793	0.007789054	0.01268977
25	0.02085648	0.006973237	0.006576569	0.009238851
26	0.01860641	0.005672865	0.005901765	0.008190883
27	0.01719889	0.005157174	0.005210118	0.007310289
28	0.0163714	0.003701681	0.004762662	0.006096475
29	0.01275484	0.003336974	0.003590122	0.005350699
30	0.01120185	0.003211909	0.002899545	0.004738032
31	0.008186426	0.002867532	0.002689219	0.004025248
32	0.007146043	0.002546928	0.002129971	0.003369917
33	0.006847521	0.001895674	0.001999959	0.00298234
34	0.005721899	0.001679872	0.001759064	0.002129302
35	0.005011147	0.001438052	0.001659869	0.001910486
36	0.00387272	0.001261306	0.001503251	0.001467214
37	0.003319498	0.000948191	0.001415628	0.001237893
38	0.002545716	0.000873997	0.00103917	0.001090832
39	0.002327433	0.000767043	0.000800442	0.0009304
40	0.002051943	0.00063325	0.000649608	0.000795323
41	0.001812613	0.0004356	0.000526748	0.000768537
42	0.001775264	0.000421136	0.000412124	0.000620146
43	0.00163802	0.000367402	0.000384948	0.000522763
44	0.001094471	0.00028586	0.000311238	0.000450129
45	0.000982014	0.000249133	0.00028321	0.000412366
46	0.000721904	0.000220998	0.000264208	0.000328771
47	0.000510986	0.000200248	0.000226573	0.000301508
48	0.000440729	0.000135051	0.000208794	0.000220335
49	0.000407382	0.000106935	0.000180361	0.00017702
50	0.000369216	8.96469E-05	0.000143228	0.00011524
51	0.000229446	8.35617E-05	0.000133855	3.587E-15
52	0.000192718	7.21176E-05	0.00010971	1.40311E-15
53	0.000164855	6.42727E-05	8.61133E-05	1.30116E-15
54	0.000130111	5.90649E-05	7.48334E-05	1.26012E-15
55	8.16214E-05	4.66983E-05	4.83977E-05	9.89834E-16
56	5.77398E-05	3.28581E-05	3.32044E-05	9.79486E-16
Total variance explained:	100	100	100	100

Table S2. Percent variance explained by each pPC

Table S3

	Average ± stdev			T-test
	Other bombycoids	Silkmoths	Hawkmoths	*p* (Silk.-Hawk.)
$\hat{r}_2$	0.528 ± 0.024	0.503 ± 0.027	0.525 ± 0.011	<0.0001
AR	1.997 ± 0.263	2.096 ± 0.190	3.237 ± 0.314	<0.0001
W_s (g•cm^{-2})	0.032 ± 0.014	0.022 ± 0.012	0.076 ± 0.034	<0.0001
S/m_t	0.002 ± 0.0007	0.003 ± 0.001	0.0008 ± 0.0003	<0.0001
$\hat{l}_{tho}$	0.3008 ± 0.059889	0.32948 ± 0.032573	0.29120 ± 0.029230	<0.0001
$\hat{l}_{abd}$	0.6351 ± 0.06688	0.61704 ± 0.04127	0.64521 ± 0.035400	0.01334
n (Hz)	22.67 ± 8.76	14.35 ± 5.21	29.374 ± 9.885	<0.0001

Table S3. Clade averaged combined wing and body measurements with corresponding statistics.

Table S4

	Average ± stdev		
	Other bombycoids	Silkmoths	Hawkmoths
R (m)	0.0349 ± 0.0172	0.0532 ± 0.0169	0.04128 ± 0.0151
$\bar{c}$ (m)	0.0179 ± 0.0095	0.0241 ± 0.00767	0.01291 ± 0.00432
S (m^2)	0.00076 ± 0.00076	0.00138 ± 0.00078	0.0006 ± 0.0004
l_b (m)	0.0272 ± 0.010591	0.02852 ± 0.007602	0.03699 ± 0.010579
l_{abd} (m)	0.0175 ± 0.007939	0.01771 ± 0.00534	0.023979 ± 0.007354
m_t (g)	0.422 ± 0.386	0.574 ± 0.408	0.972 ± 0.849
P_{acc}	25.157 ± 5.831	21.7934 ± 4.9644	38.4479 ± 8.779

Table S4. Additional clade averaged combined wing and body measurements that were not critical to this study, but, because of their functional relevance, could be useful for future studies.

			Measured masses (g)			Wing area (m^2)		Mass estimations (g)			Absolute percent error of estimation			Percent error of estimation		
Species	Family	Sex	Body	Forewing	Hindwing	Forewing	Hindwing	Body mass	Forewing	Hindwing	Body mass	Forewing mass	Hindwing mass	Body mass	Forewing mass	Hindwing mass
Amphion floridensis	Sphingidae	F	0.5066	0.005	0.001	0.000132261	8.74E-05	0.652499492	0.004735	0.00158415	0.287997418	0.052945247	0.584147371	-0.287997418	0.052945247	-0.584147371
Antheraea godmani	Saturniidae	M	1.509	0.135	0.071	0.002272542	0.00173893	1.62629868	0.073591	0.03864964	0.077732723	0.454878552	0.455638896	-0.077732723	0.454878552	0.455638896
Antheraea godmani	Saturniidae	M	3.5079	0.063	0.0277	0.002006188	0.001257508	2.28479764	0.065253	0.02733929	0.348670817	0.035755951	0.013021884	0.348670817	-0.035755951	0.013021884
Antheraea godmani	Saturniidae	M	3.5585	0.0777	0.0376	0.001839901	0.00105612	2.173179533	0.060027	0.02268967	0.389298993	0.227450818	0.396551222	0.389298993	0.227450818	0.396551222
Antheraea godmani	Saturniidae	M	3.2836	0.0587	0.0269	0.001905864	0.001493434	1.578719037	0.062102	0.03285096	0.519210916	0.057953587	0.221225162	0.519210916	-0.057953587	-0.221225162
Automeris io	Saturniidae	M	0.4518	0.0105	0.0075	0.000384114	0.000394244	0.378744146	0.013244	0.00792022	0.161699544	0.261360959	0.056028841	0.161699544	-0.261360959	-0.056028841
Automeris io	Saturniidae	M	0.2324	0.0075	0.0048	0.000255542	0.000301172	0.361985901	0.008939	0.00594047	0.557598542	0.191838823	0.237598854	-0.557598542	-0.191838823	-0.237598854
Automeris io	Saturniidae	M	0.3132	0.0103	0.0056	0.000303055	0.000304185	0.40423533	0.010537	0.00600399	0.290661972	0.02302702	0.072141702	-0.290661972	-0.02302702	-0.072141702
Automeris io	Saturniidae	F	0.713	0.014	0.009	0.000525351	0.00041513	0.729002486	0.017915	0.00836918	0.022443879	0.279645431	0.070090959	-0.022443879	-0.279645431	0.070090959
Automeris io	Saturniidae	F	0.817	0.0155	0.01	0.000450209	0.000407517	0.738752928	0.015436	0.00820534	0.09577365	0.004097775	0.179465546	0.09577365	0.004097775	0.179465546
Automeris io	Saturniidae	F	0.426	0.009	0.0055	0.000390831	0.000323383	0.382256883	0.013468	0.00640958	0.102683374	0.496407212	0.165377904	0.102683374	-0.496407212	-0.165377904
Automeris io	Saturniidae	F	0.472	0.011	0.008	0.000358393	0.000282433	0.540800052	0.012388	0.00554654	0.145762821	0.126155909	0.306682589	-0.145762821	-0.126155909	0.306682589
Amorpha juglandis	Sphingidae	F	0.1787	0.0055	0.0013	0.00016112	0.000127284	0.347164809	0.005728	0.00236761	0.942724169	0.041537913	0.821240435	-0.942724169	-0.041537913	-0.821240435
Actias luna	Saturniidae	M	0.4784	0.0332	0.0208	0.000864174	0.000713445	0.546835491	0.028956	0.01492363	0.143050775	0.127830404	0.282517695	-0.143050775	0.127830404	0.282517695
Actias luna	Saturniidae	F	2.4838	0.0531	0.03	0.001453067	0.00133423	1.912258121	0.047803	0.02912453	0.230107851	0.099751572	0.029182375	0.230107851	0.099751572	0.029182375
Actias luna	Saturniidae	M	0.8278	0.0426	0.0295	0.001083046	0.001051253	0.737083997	0.036002	0.02257801	0.10958686	0.154887965	0.234643681	0.10958686	0.154887965	0.234643681
Actias luna	Saturniidae	M	1.0116	0.0537	0.0355	0.001155174	0.001183752	1.032769429	0.038312	0.02563006	0.02092668	0.286553359	0.278026354	-0.02092668	0.286553359	0.278026354
Actias luna	Saturniidae	F	0.2737	0.014	0.0067	0.000543059	0.000463288	0.450550314	0.018497	0.00941012	0.64614656	0.321231613	0.404495702	-0.64614656	-0.321231613	-0.404495702
Actias maenas	Saturniidae	F	3.641	0.0502	0.0608	0.002884743	0.002707167	2.661988651	0.092633	0.06201109	0.268885292	0.845277506	0.019919313	0.268885292	-0.845277506	-0.019919313
Automeris metzli	Saturniidae	F	1.543	0.0355	0.019	0.001013569	0.000900741	1.209914175	0.033771	0.01914292	0.215868973	0.048697938	0.007521861	0.215868973	0.048697938	-0.007521861
Automeris metzli	Saturniidae	M	0.8278	0.0428	0.0233	0.000938764	0.00093591	0.940723473	0.031364	0.0199423	0.136413956	0.267207109	0.144107238	-0.136413956	0.267207109	0.144107238
Automeris metzli	Saturniidae	M	0.7303	0.0372	0.019	0.000835567	0.000853852	0.934387526	0.028031	0.01808047	0.279457108	0.246484368	0.048396533	-0.279457108	0.246484368	0.048396533
Anisota pellucida	Saturniidae	F	0.4754	0.0077	0.0026	0.000220114	0.000106248	0.356716167	0.00774	0.00195215	0.249650469	0.005220061	0.249171664	0.249650469	-0.005220061	0.249171664
Anisota pellucida	Saturniidae	F	0.5564	0.009	0.0028	0.000273917	0.000132686	0.479358148	0.009558	0.00247508	0.138464867	0.062008853	0.116044093	0.138464867	-0.062008853	0.116044093
Anisota pellucida	Saturniidae	M	0.2328	0.0042	0.001	0.000113096	6.91E-05	0.18314462	0.004072	0.00123381	0.213296307	0.030579475	0.233813795	0.213296307	0.030579475	-0.233813795
Anisota pellucida	Saturniidae	F	0.4892	0.0086	0.0023	0.000269004	0.00014277	0.356224835	0.009393	0.00267651	0.271821678	0.092170511	0.163700219	0.271821678	-0.092170511	-0.163700219
Anisota pellucida	Saturniidae	F	0.4806	0.0094	0.0028	0.000237363	0.000161098	0.342717634	0.008325	0.00304504	0.286896308	0.114408451	0.087513602	0.286896308	0.114408451	-0.087513602
Anisota pellucida	Saturniidae	F	0.497	0.0076	0.0025	0.000272774	0.000162614	0.437905086	0.00952	0.00307565	0.118903247	0.252580988	0.230260633	0.118903247	-0.252580988	-0.230260633
Callosamia angulifera	Saturniidae	M	0.3667	0.018	0.008	0.000781554	0.000647813	0.234663295	0.026281	0.01346199	0.36006737	0.460041812	0.68274853	0.36006737	-0.460041812	-0.68274853
Callosamia angulifera	Saturniidae	M	0.38	0.023	0.012	0.000964885	0.00095782	0.334532155	0.032205	0.02044134	0.119652222	0.400218473	0.703444727	0.119652222	-0.400218473	-0.703444727
Callosamia angulifera	Saturniidae	F	0.8382	0.0183	0.0101	0.000996316	0.000855563	0.47465223	0.033216	0.01811917	0.433724373	0.815108699	0.793977361	0.433724373	-0.815108699	-0.793977361
Eumorpha achemon	Sphingidae	F	1.0768	0.015	0.0061	0.000443857	0.000254444	1.377370303	0.015226	0.0049615	0.279132896	0.015088507	0.186639905	-0.279132896	-0.015088507	0.186639905
Eupackardia calleta	Saturniidae	M	0.5936	0.03	0.0172	0.000867567	0.000793465	0.599965867	0.029066	0.01671805	0.010724169	0.031142673	0.028020331	-0.010724169	0.031142673	0.028020331
Eupackardia calleta	Saturniidae	F	1.327	0.031	0.018	0.000929637	0.000847236	1.021894895	0.031069	0.01793086	0.229920954	0.002236285	0.003840845	0.229920954	-0.002236285	0.003840845
Eupackardia calleta	Saturniidae	F	1.274	0.037	0.021	0.000948929	0.000807296	1.158047781	0.031691	0.0170295	0.091014301	0.143483269	0.189071417	0.091014301	0.143483269	0.189071417
Eupackardia calleta	Saturniidae	F	1.3357	0.0316	0.0175	0.001032686	0.000893712	0.995904631	0.034385	0.01898341	0.254394975	0.08814805	0.084766179	0.254394975	-0.08814805	-0.084766179
Eupackardia calleta	Saturniidae	M	0.541	0.0283	0.0159	0.00081206	0.000697497	0.463946728	0.02727	0.01456759	0.142427489	0.036408228	0.083799542	0.142427489	0.036408228	0.083799542
Eacles imperialis	Saturniidae	M	1.9039	0.071	0.0372	0.001032399	0.000950291	2.409113311	0.034376	0.02026976	0.265357062	0.515827204	0.455114098	-0.265357062	0.515827204	0.455114098
Hyalophora cecropia	Saturniidae	M	1.4848	0.068	0.0406	0.002102342	0.00190799	1.325326713	0.068267	0.04267596	0.107403884	0.003928835	0.051131918	0.107403884	-0.003928835	-0.051131918
Hyalophora cecropia	Saturniidae	F	3.1715	0.072	0.04	0.002325637	0.001918955	2.200530105	0.075249	0.04293797	0.306154783	0.045130345	0.073449199	0.306154783	-0.045130345	-0.073449199
Hyalophora cecropia	Saturniidae	F	3.142	0.071	0.041	0.002046114	0.002032696	2.648021892	0.066505	0.04566172	0.15721773	0.063310409	0.113700491	0.15721773	0.063310409	-0.113700491
Hyalophora cecropia	Saturniidae	M	1.3914	0.074	0.0468	0.001964682	0.001915263	1.595212967	0.06395	0.04284975	0.1464805	0.135813687	0.084407145	-0.1464805	0.135813687	0.084407145
Hyalophora cecropia	Saturniidae	F	2.3638	0.071	0.0405	0.002060021	0.001693071	2.093807909	0.066941	0.03756192	0.114219516	0.057169582	0.07254509	0.114219516	0.057169582	0.07254509
Hyalophora cecropia	Saturniidae	M	1.3136	0.0602	0.032	0.001699646	0.001577317	1.424005352	0.055607	0.03482549	0.084047923	0.076301256	0.08829655	-0.084047923	0.076301256	-0.08829655
Hyalophora euryalus	Saturniidae	F	1.0244	0.021	0.0196	0.000984424	0.000804744	0.844638299	0.032834	0.01697199	0.175479989	0.563520975	0.134081946	0.175479989	-0.563520975	0.134081946
Hyalophora euryalus	Saturniidae	M	3.1518	0.0296	0.02	0.0011915	0.00124459	0.788911112	0.039474	0.02703943	0.749695059	0.333571208	0.351971541	0.749695059	-0.333571208	-0.351971541
Hyalophora euryalus	Saturniidae	M	1.8074	0.0341	0.0222	0.000966091	0.00110034	1.133842052	0.032244	0.02370581	0.372666786	0.054432754	0.067829199	0.372666786	0.054432754	-0.067829199
Hyalophora euryalus	Saturniidae	M	1.3062	0.0382	0.0237	0.001199047	0.00116587	1.292587333	0.039715	0.02521675	0.01042158	0.039656896	0.063997993	0.01042158	-0.039656896	-0.063997993
Hyalophora euryalus	Saturniidae	M	1.3016	0.0334	0.0211	0.001379117	0.000973977	1.292108265	0.045454	0.02080985	0.007292359	0.360901568	0.013750992	0.007292359	-0.360901568	0.013750992
Hyalophora euryalus	Saturniidae	F	2.0648	0.0354	0.0247	0.001426334	0.001233134	1.796550481	0.046954	0.02677368	0.129915497	0.326397993	0.083954629	0.129915497	-0.326397993	-0.083954629
Manduca rustica	Sphingidae	F	3.2057	0.057	0.0172	0.000901594	0.000539943	4.350026309	0.030165	0.01108207	0.356966126	0.470794537	0.355693697	-0.356966126	0.470794537	0.355693697
Prosperinus clarkiae	Sphingidae	M	0.1406	0.0025	0.0013	7.06E-05	4.78E-05	0.291490345	0.002584	0.00083202	1.073188801	0.033671513	0.359987605	-1.073188801	-0.033671513	0.359987605
Paonias myops	Sphingidae	F	0.3933	0.0051	0.0013	0.000194433	0.000154929	0.499067238	0.006867	0.00292066	0.268922549	0.346502655	1.246665252	-0.268922549	-0.346502655	-1.246665252
Rothschildia cincta	Saturniidae	F	1.5974	0.0423	0.0269	0.001408909	0.001388426	1.275150162	0.046401	0.03038984	0.201733966	0.096950514	0.129733957	0.201733966	-0.096950514	-0.129733957
Rothschildia cincta	Saturniidae	M	1.3614	0.033	0.0203	0.001019893	0.0010554	0.890555965	0.033974	0.02267315	0.345852824	0.029529237	0.116904044	0.345852824	-0.029529237	-0.116904044
Rothschildia cincta	Saturniidae	M	1.2758	0.033	0.0208	0.001185932	0.001170048	1.230075347	0.039296	0.02531327	0.035839985	0.190780362	0.216984075	0.035839985	-0.190780362	-0.216984075
Rothschildia cincta	Saturniidae	F	1.6678	0.0401	0.025	0.001190041	0.001159993	1.28595051	0.039427	0.025081	0.228954005	0.016780855	0.003240152	0.228954005	0.016780855	-0.003240152
Rothschildia cincta	Saturniidae	M	1.2608	0.0313	0.0179	0.001268987	0.001030161	1.138697919	0.041947	0.02209449	0.096844925	0.340172957	0.234328878	0.096844925	-0.340172957	-0.234328878
Rothschildia cincta	Saturniidae	M	1.6652	0.0495	0.03	0.001134858	0.00125882	1.112612384	0.037662	0.02736977	0.331844593	0.239153766	0.08767421	0.331844593	0.239153766	0.08767421
Samia cynthia	Saturniidae	M	0.5029	0.0417	0.0216	0.001273527	0.001125948	0.476524434	0.042092	0.02429555	0.05244694	0.0094044	0.124793753	0.05244694	-0.0094044	-0.124793753
Samia cynthia	Saturniidae	M	0.9064	0.045	0.0253	0.001716227	0.001483821	0.976147083	0.05613	0.03262515	0.076949562	0.247330762	0.289531697	-0.076949562	-0.247330762	-0.289531697
Samia cynthia	Saturniidae	M	0.2204	0.02	0.01	0.000896287	0.000854661	0.261993594	0.029993	0.01809877	0.188718665	0.499670497	0.809877478	-0.188718665	-0.499670497	-0.809877478
Sphinx kalmiae	Sphingidae	F	1.292	0.0188	0.006	0.000446478	0.0002623	1.236646495	0.015313	0.00512528	0.04284327	0.185475778	0.145785901	0.04284327	0.185475778	0.145785901
Sphinx kalmiae	Sphingidae	F	0.6745	0.015	0.0042	0.000328485	0.000194642	0.913006642	0.011389	0.00372677	0.353605102	0.240738274	0.1126731	-0.353605102	0.240738274	0.1126731
Sphinx kalmiae	Sphingidae	M	1.1874	0.0208	0.007	0.000496541	0.000295346	1.144275337	0.016966	0.00581782	0.036318564	0.184310292	0.168882535	0.036318564	0.184310292	0.168882535
Sphinx kalmiae	Sphingidae	M	1.0003	0.0206	0.0069	0.000408106	0.000292949	1.145314816	0.014041	0.0057674	0.144971325	0.318374976	0.164144935	-0.144971325	0.318374976	0.164144935
Sphinx kalmiae	Sphingidae	M	0.8124	0.018	0.0068	0.000394609	0.000218997	1.341715313	0.013593	0.0042269	0.651545191	0.244821007	0.378397284	-0.651545191	0.244821007	0.378397284
Sphinx kalmiae	Sphingidae	F	1.4186	0.0242	0.007	0.000503142	0.000261407	1.617194751	0.017184	0.00510665	0.13999348	0.289922697	0.270478662	-0.13999348	0.289922697	0.270478662
Sphinx kalmiae	Sphingidae	F	1.4434	0.0219	0.0068	0.000449645	0.000261683	1.369762094	0.015418	0.00511241	0.051016978	0.295989062	0.248175278	0.051016978	0.295989062	0.248175278
Sphinx kalmiae	Sphingidae	F	0.9378	0.0201	0.006	0.000389964	0.000224281	1.250175874	0.013439	0.00433593	0.333094342	0.331402165	0.277345222	-0.333094342	0.331402165	0.277345222
Smerinthus ophthalmica	Sphingidae	M	0.8388	0.0092	0.0032	0.000323853	0.000184612	0.754727255	0.011234	0.00352203	0.100229787	0.221080899	0.100633136	0.100229787	-0.221080899	-0.100633136
Average			1.232135211	0.032559155	0.01804507	0.000947884	0.000814735	1.082362791	0.031415	0.01752406	23.85%	20.58%	23.04%	1.52%	-3.54%	-4.38%
Standard deviation			0.920477456	0.023937834	0.014641348	0.000640935	0.000586414	0.728431	0.020591	0.01328458	20.55%	18.56%	23.13%	31.57%	27.59%	32.46%

Table S5: Estimation of body and wing mass

Trait	mean MDI	MDI stdev	p-value
Forewing	-0.037851	0.10072	0.304
Hindwing	0.014947	0.126758	0.518
Combined wing	0.006025	0.133396	0.485
AR	-0.221745	0.201691	0.022
Radius of the 2nd moment of area	0.385852	0.192508	0.943
Relative wing area	-0.033261	0.194523	0.347
Wing beat frequency	-0.007048	0.202154	0.412
Wing loading	-0.026998	0.195977	0.359

Table S6: MDI results of the DTT analysis

Table S7.

	1 regime			2 regime		2 regime		3 regimes		Multi
				Silkmoths different		Hawkmoths different		Each group different		P.EM
Model:	BM	OU	EB	BM	OU	BM	OU	BM	OU	--
	Aicc (#P)	Aicc (#P)	Aicc (#P)	Aicc (#P)	Aicc (#P)	Aicc (#P)	Aicc (#P)	Aicc (#P)	Aicc (#P)	Aicc (#P)
cw	-121.212 (5)	-141.098 (8)	-118.982 (6)	-214.123 (8)	-141.247 (10)	-183.184 (3)	-155.311 (10)	-213.018 (11)	-152.872 (12)	-379.87 (18)
$\hat{r}_2$	-250.7 (2)	-262.489 (3)	-248.47 (3)	-266.238 (3)	-263.216 (4)	-258.579 (3)	-260.45 (4)	-264.218 (4)	-260.928 (5)	-291.401 (4)
AR	53.60306 (2)	54.70865 (3)	55.83367 (3)	47.57168 (3)	54.93009 (4)	45.02165 (3)	16.17843 (4)	47.33685 (4)	17.72989 (5)	16.17843 (4)
W_s	-238.303 (2)	-242.32 (3)	-236.073 (3)	-259.283 (3)	-244.483 (4)	-272.649 (3)	-252.189 (4)	-271.943 (4)	-255.244 (5)	-329.848 (13)
n	401.5512 (2)	401.7321 (3)	403.7818 (3)	395.8774 (3)	399.8752 (4)	391.9343 (3)	400.6526 (4)	394.2245 (4)	400.3504 (5)	370.0447 (6)
S/m_t	-635.221 (2)	-636.6 (3)	-632.99 (3)	-633.242 (3)	-638.4 (4)	-632.99 (3)	-639.775 (4)	-630.676 (4)	-641.14 (5)	-670.458 (6)

Table S7: Comparison of the fit of evolutionary models for each wing trait.
Symbols can be found in Table S1.

Tip Name	Family	Genus	Species	Data	Dataset	Recovery
_Acti	Saturniidae	Actias	luna	transcriptome	Kawahara & Breinholt 2014	776
_MSEXT	Sphingidae	Manduca	sexta	transcriptome	Kawahara & Breinholt 2014	790
247279219_Sphingidae_Smerinthinae_Polyptychus-Genus-Group_x_Polyptychus_trilineatus_x	Sphingidae	Polyptychus	trilineatus	AHE	NEW	244
2Sphingidae_Sphingidae_Smerinthinae_Polyptychus-Genus-Group_x_Pseudoclanis_postica_x	Sphingidae	Pseudoclanis	postica	AHE	NEW	496
AD3153_Sphingidae_Andriasa_contraria	Sphingidae	Andriasa	contraria	AHE	Hamilton et al., 2019	720
ADW1522_Saturniidae_Hemileucinae_Hemileuca_magnifica	Saturniidae	Hemileuca	magnifica	AHE	Hamilton et al., 2019	402
AYK140002_Saturniidae_Antheraea_polyphemus	Saturniidae	Antheraea	polyphemus	AHE	Rubin & Hamilton et al., 2018	750
CAH0104_Saturniidae_Saturniinae_Attacini_x_Callosamia_angulifera_x	Saturniidae	Callosamia	angulifera	AHE	NEW	564
DNAAZ27_Anthelidae_Anthelinae_Anthela_ocellata	Anthelidae	Anthela	ocellata	AHE	Hamilton et al., 2019	442
DT2557_Sphingidae_Dolbina_tancrei	Sphingidae	Dolbina	tancrei	AHE	Hamilton et al., 2019	774
Ffaa_Sphingidae_Falcatula_falcata	Sphingidae	Falcatula	falcata	AHE	Hamilton et al., 2019	761
HL1881_Sphingidae_Hyles_lineata	Sphingidae	Hyles	lineata	AHE	NEW	761
I3503_Saturniidae_Eacles_imperialis_or_ormondei	Saturniidae	Eacles	imperialis	AHE	Hamilton et al., 2019	738
I3504_Saturniidae_Samia_tetrica	Saturniidae	Samia	tetrica	AHE	Rubin & Hamilton et al., 2018	753
I3508_Saturniidae_Actias_maenas	Saturniidae	Actias	maenas	AHE	Rubin & Hamilton et al., 2018	766
I3511_Sphingidae_Coequosa_triangularis	Sphingidae	Coequosa	triangularis	AHE	Hamilton et al., 2019	766
I3518_Sphingidae_Pachysphinx_occidentalis	Sphingidae	Pachysphinx	imperator	AHE	NEW	776
I3519_Sphingidae_Sphinx_chersis	Sphingidae	Sphinx	chersis	AHE	Hamilton et al., 2019	775
I3523_Laophontidae_Langia_zenzeroides	Sphingidae	Langia	zenzeroides	AHE	Hamilton et al., 2019	763
I3524_Sphingidae_Mimas_tiliae	Sphingidae	Mimas	tiliae	AHE	NEW	780
I3528_Sphingidae_Amphion_floridensis	Sphingidae	Amphion	floridensis	AHE	NEW	766
I3530_Sphingidae_Pseudosphinx_UNKNOWN	Sphingidae	Pseudosphinx	tetrio	AHE	Hamilton et al., 2019	771
LEP-43120_Lasiocampidae_Lasiocampinae_Lasiocampini_x_Prorifrons_sp_x	Lasiocampidae	Prorifrons	sp	AHE	NEW	497
LEP-44917_Saturniidae_Ceratocampinae_x_x_Citheronia_sepulcralis_x	Saturniidae	Citheronia	sepulcralis	AHE	NEW	567
LEP-52739_Bombycidae_Bombycinae_x_x_Bombyx_mandarina_x	Bombycidae	Bombyx	mandarina	AHE	NEW	586
LEP-62244_Saturniidae_Agliinae_x_x_Aglia_tau_x	Saturniidae	Aglia	tau	AHE	NEW	565
LEP12192_Sphingidae_Ambulyx_canescens	Sphingidae	Ambulyx	canescens	AHE	Hamilton et al., 2019	723
LEP12513_Sphingidae_Macroglossinae_Macroglossum_sylvia	Sphingidae	Macroglossum	sylvia	AHE	Hamilton et al., 2019	532
LEP12527_Sphingidae_Callambulyx_amanda	Sphingidae	Callambulyx	amanda	AHE	Hamilton et al., 2019	741
LEP12973_Sphingidae_Smerinthinae_Clanis_undulosa	Sphingidae	Clanis	undulosa	AHE	Hamilton et al., 2019	595
LEP14056_Sphingidae_Smerinthinae_Paonias_myops	Saturniidae	Paonias	myops	AHE	NEW	618
LEP14171_Sphingidae_Macroglossinae_Deilephila_elpenor	Sphingidae	Deilephila	elpenor	AHE	NEW	589
LEP14407_Sphingidae_Macroglossinae_Eumorpha_achemon	Saturniidae	Eumorpha	achemon	AHE	NEW	597
LEP21041_Sphingidae_Smerinthinae_Polyptychus_andosa	Sphingidae	Polyptychus	andosa	AHE	Hamilton et al., 2019	548
LEP23372_Sphingidae_Smerinthinae_Smerinthus_jamaicensis	Sphingidae	Smerinthus	jamaicensis	AHE	Hamilton et al., 2019	605
LEP24256_Bombycidae_Apatelodes_firmiana	Apatelodidae	Apatelodes	firmiana	AHE	Hamilton et al., 2019	703
LEP24348_Phiditiidae_unknown_Phiditia_sp	Phiditiidae	Phiditia	sp	AHE	NEW	547
LEP24721_Saturniidae_Hemileucinae_Automeris_janus	Saturniidae	Automeris	janus	AHE	NEW	614
LEP28601_Saturniidae_Rothschildia_lebeau	Saturniidae	Rothschildia	lebeau	AHE	Rubin & Hamilton et al., 2018	533
LEP29044_Saturniidae_Arsenura_armida	Saturniidae	Arsenura	armida	AHE	Rubin & Hamilton et al., 2018	766
LEP32277d_Saturniidae_Bunaea_alcinoe	Saturniidae	Bunaea	alcinoe	AHE	Rubin & Hamilton et al., 2018	702
LEP36752_Sphingidae_Macroglossinae_Hemaris_thysbe	Sphingidae	Hemaris	thysbe	AHE	Hamilton et al., 2019	592
LEP39332_Saturniidae_Saturniinae_Hyalophora_colombia	Saturniidae	Hyalophora	colombia	AHE	NEW	542
LEP39470_Saturniidae_Ceratocampinae_Anisota_pellucida	Saturniidae	Anisota	pellucida	AHE	Hamilton et al., 2019	585
LEP40497_Saturniidae_Saturniinae_Actias_philippinica	Saturniidae	Actias	philippinica	AHE	Rubin & Hamilton et al., 2018	570
LEP41075_Saturniidae_Eudaemonia_agriphontes	Saturniidae	Eudaemonia	agriphontes	AHE	Rubin & Hamilton et al., 2018	760
LEP41093_Saturniidae_Salassa_sp	Saturniidae	Salassa	sp	AHE	Rubin & Hamilton et al., 2018	748
LEP41811_Saturniidae_Cercophaninae_Cercophana_venusta	Saturniidae	Cercophana	venusta	AHE	Hamilton et al., 2019	598
LEP43920_Saturniidae_Saturniinae_Micragone_agathylla	Saturniidae	Micragone	agathylla	AHE	Rubin & Hamilton et al., 2018	561
LEP47817_Saturniidae_Hemileucinae_Polythysana_cinerascens	Saturniidae	Polythysana	cinerascens	AHE	Hamilton et al., 2019	525
RROU00221_Brahmaeidae_Acanthobrahmaea_europaea_sp	Brahmaeidae	Brahmaea	europaea	AHE	Hamilton et al., 2019	502
RSP951002_Endromidae_Endromis_versicolora	Endromidae	Endromis	versicolora	AHE	Hamilton et al., 2019	769
RSPxx1045_Saturniidae_Actias_artemis	Saturniidae	Actias	artemis	AHE	Rubin & Hamilton et al., 2018	764
S1C1R3D_Saturniidae_Saturniinae_Saturnia-Eudia_pavonia	Saturniidae	Saturnia	pavonia	AHE	Hamilton et al., 2019	588
SMNSDNALEP293_Eupterotidae_Janinae_Jana_preciosa	Eupterotidae	Jana	preciosa	AHE	Hamilton et al., 2019	575
SW130019T_Sphingidae_Smerinthinae_Smerinthini_Marumba_sp	Sphingidae	Marumba	sp	transcriptome	NEW	719
V005T_Sphingidae_Smerinthinae_Smerinthini_Parum_colligata	Sphingidae	Parum	colligata	transcriptome	NEW	723

Table S8. Tip names and data source of each species in phylogeny

Species	N Females	N Males	N Total
Anthela_sp	1	0	1
Apatelodes_torrefacta	0	3	3
Bombyx_mandarina	0	2	2
Brahmaea_paratypus	0	1	1
Endromis_versicolora	0	2	2
Jana_eurymas	0	2	2
Lasiocampa_terreni	0	2	2
Phiditia_lucernaria	0	2	2
Actias_artemis	0	2	2
Actias_dubernardi	0	2	2
Actias_luna	0	2	2
Actias_maenas	0	2	2
Aglia_tau	0	3	3
Anisota_stigma	1	0	1
Antheraea_polyphemus	0	5	5
Arsenura_a_armida	0	3	3
Automeris_io	0	2	2
Bunaea_alcinoe	0	2	2
Callosamia_angulifera	0	5	5
Cercophana_venusta	0	2	2
Citheronia_sepulcralis	0	2	2
Eacles_imperialis	0	3	3
Eudaemonia_agriphontes	0	3	3
Hemileuca_magnifica	0	3	3
Hyalophora_euryalus	0	3	3
Micragone_bilineata	0	1	1
Polythysana_cinerascens	0	2	2
Rothschildia_lebeau	0	4	4
Salassiinae_salassa	0	3	3
Samia_cynthia	0	5	5
Saturnia_pavonia	0	3	3
Ambulyx_canescus	0	2	2
Amphion_floridensis	0	2	2
Andriasa_contraria	0	2	2
Callambulyx_amanda	0	1	1
Clanis_undulosa	0	2	2
Coequosa_triangularis	1	0	1
Deilephila_elpenor	0	2	2
Dolbina_tancrei	0	2	2
Eumorpha_achemon	0	2	2
Falcatula_falcatus	0	1	1
Hemaris_thetis	0	1	1
Hyles_lineata	0	2	2
Langia_zenzeroides	0	2	2
Macroglossum_stellatarum	0	1	1
Manduca_sexta	0	2	2
Marumba_gaschkewitschii	0	2	2
Mimas_tiliae	0	2	2
Pachysphinx_modesta	0	3	3
Paonias_myops	0	3	3
Parum_colligata	0	2	2
Polyptychus_andosa	0	2	2
Polyptychus_trilineatus	0	2	2
Pseudoclanis_postica	0	2	2
Pseudosphinx_tetrio	0	2	2
Smerinthus_ophthalmica	2	0	2
Sphinx_chersis	0	2	2

Table S9. Sex and count of individuals used in shape analysis for each species